Metastable domains and potential energy surfaces in organic charge-transfer salts with neutral-ionic phase transitions

Zoltán G. Soos[1,*] and Anna Painelli[2,†]
[1]*Department of Chemistry, Princeton University, Princeton, New Jersey 08544, USA*
[2]*Dipartimento Chimica GIAF, Parma University, & INSTM UdR Parma, 43100 Parma, Italy*
(Received 29 January 2007; published 27 April 2007)

A modified Hubbard model with linear coupling to both lattice phonons and molecular vibrations is applied to the structural and electronic instabilities of organic charge-transfer (CT) salts such as tetrathiafulvalene-chloranil (TTF-CA). The potential energy surface (PES) of the correlated model is found exactly in finite one-dimensional (1D) systems with a mean-field approximation for 3D Coulomb interactions and parameters close to first or second-order phase transitions. The PES near a first-order transition has multiple minima with different values of ρ, the degree of CT in the ground state. The energy of metastable domains is related to their length L, to the discontinuity $\Delta\rho$ at the transition, and to the energy $2E_w$ of two domain walls. Sharp and relaxed domain walls are modeled by free spinless fermions coupled to both phonons and molecular vibrations whose ground-state PES is obtained in chains of up to 1000 sites. When $\Delta\rho$ is sufficiently small, metastable domains become thermally accessible at low temperature where the Boltzmann population of electronic excitations is negligible. The pressure-induced transition of TTF-CA is discussed in terms of an equilibrium between stable and metastable domains with different ρ, using previous parameters for the temperature-induced transition, where metastable domains are not accessible thermally. In either correlated or uncorrelated models, linear coupling of electrons to slow, harmonic coordinates for lattice and molecular vibrations leads to strongly anharmonic PES near an electronic or structural instability. CT salts with neutral-ionic transitions illustrate competition between a lattice phonon that drives a second-order Peierls transition and molecular vibrations that favor a first-order $\Delta\rho$.

DOI: 10.1103/PhysRevB.75.155119 PACS number(s): 71.10.Fd, 63.20.Kr, 73.43.Nq, 71.30.+h

I. INTRODUCTION

The rich phase diagram of models for correlated electrons in reduced dimensions is due to competition between the kinetic energy that favors electronic delocalization and electrostatic interactions or disorder that favor localization. The one-dimensional (1D) Hubbard model is a familiar case. The relative strength of on-site and intersite electron-electron (e-e) interactions leads to different phases at $T=0$ K and governs the nature of the boundary between the phases.[1–3] Even more complex 0-K phase diagrams occur in 1D models with nonequivalent sites or in 2D models with stripe formation. Indeed, 2D models for cuprates, manganites, or organic superconductors are extremely complex and point to multiple electronic structures that are almost degenerate.[4] Interesting physics emerges in these materials as a result of competing interactions and phases: phase coexistence and quantum phase transitions are some of the most striking manifestations of soft behavior, defined in terms of the possibility to alter the state of the material by the application of minor external stimuli.[4]

The modified Hubbard model has alternating site energies in 1D and several competing phases and interactions. The continuous crossover from a band to a Mott insulator shows an unusual interplay between spin and charge degrees of freedom[5–8] with important consequences on the polarization and polarizability.[8–10] Intersite e-e interactions affect the nature of optical excitations,[11–13] as well as the nature of the interface, driving a discontinuous phase crossover.[5,7,14,15] The modified Hubbard model represents the standard microscopic model for organic charge-transfer (CT) salts with a mixed stack motif of π-electron donors (D) and acceptors (A), some of which exhibit a neutral-ionic phase transition (NIT).[16–18] The complex phenomenology of NIT offers unique opportunities for validating theoretical models. CT salts with either continuous or discontinuous NIT have indeed been observed.[17] There are large dielectric anomalies,[19] the limit of a quantum phase transition has been attained,[20] and photoinduced phase transitions support a picture of multielectron transfer for optical excitations.[12,13]

To capture NIT physics fully, however, models of electronic structure must be extended to include electron-phonon (e-ph) coupling. Lattice dimerization always accompanies NIT,[17] and Peierls coupling to a lattice phonon was recognized from the beginning.[7,21,22] In addition, there is ample experimental evidence in CT salts for strong coupling of electrons to molecular vibrations.[7,22,23] Such e-mv or Holstein coupling has a role similar to e-e interactions in favoring a discontinuous NIT.[7,10,22,23] We will consider both e-ph and e-mv coupling in correlated models close to the NIT.

Both theoretical[24,25] and experimental evidence[26] suggest that electron correlation amplifies e-ph coupling or, more generally, that the effects of coupling to vibrations are amplified near phase transitions.[9] For example, Peierls coupling near the NIT leads to the appearance of a soft mode with a huge intensity in far-infrared spectra[9] that is responsible for the dielectric anomaly at the NIT.[10,27] The soft mode has been clearly recognized in combination bands with molecular vibrations that appear in midinfrared spectra.[28] On the other hand, e-mv coupling is responsible for an anomalous softening of vibrational frequencies of totally symmetric molecular vibrations, observed in Raman spectra and, in dimerized stacks, for the appearance of so-called vibronic bands in midinfrared spectra.[29,30] In fact, e-mv coupling has primarily

been studied to extract structural information from vibrational spectra.[17,30,31]

In this paper, we model phase coexistence near the NIT by exploiting the fundamental role of vibrations. Either lattice or molecular vibrations are slow degrees of freedom that adiabatically follow electronic motions. The calculation of the ground-state (g.s.) energy of the coupled system as a function of the vibrational coordinates leads to the definition of the g.s. potential energy surface (PES) whose minima unambiguously define *stable* states. A g.s. PES with multiple minima is then a clear signature of multistability and is a prerequisite for the coexistence of several phases. Coexistence at the NIT has been proposed previously[21,31,32] and has recently been invoked to explain a variety of experimental results.[33–36] We discuss here the theoretical requirements for coexistence in terms of g.s. potentials.

TTF-CA (tetrathiafulvalene-chloranil) is the prototypical CT salt with a mixed stack, and its NIT has been studied under different conditions. It is a rare crystal with a temperature-induced NIT[16,17,31] at 81 K as well as a photo-induced NITs.[37,38] These transitions demonstrate a delicate balance between a neutral regular and an ionic dimerized g.s. TTF-CA also has a pressure-induced NIT at ambient T with a prominent coexistence region from 0.87 to 1.22 GPa, as inferred from vibrational spectra.[35,39] Accordingly, we illustrate e-ph and e-mv coupling near the NIT with parameters based on TTF-CA.

The paper is organized as follows. Section II presents a modified Hubbard model with strong e-e correlation and both e-ph and e-mv coupling. A mean-field (MF) approximation is introduced for 3D e-e interactions, and PES are computed in finite systems of 14 and 16 sites in the vicinity of either a first-order (discontinuous) or a second-order (continuous) transition. In Sec. III, we analyze a related model of free spinless fermions to study metastable domains and domain walls in extended systems of 1000 sites. Relaxation of walls along the molecular coordinate is contrasted with relaxation along the lattice coordinate, as done in the Su-Schrieffer-Heeger (SSH) model[40] of polyacetylene. The pressure-induced NIT of TTF-CA is modeled in Sec. IV in terms of metastable domains that are thermally accessible at low T where the equilibrium population of excited states is negligible. The concluding Discussion makes contact with Nagaosa and Takimoto's influential papers of neutral-ionic domain walls (NIDWs) in TTF-CA.[6,14,21,32] The present work focuses on metastable domains whose excitation is governed by length rather than by walls. We emphasize the role of slow nuclear degrees of freedom that make it possible to compute the entire PES instead of just its minima.

II. MULTISTABILITY IN CORRELATED MODELS FOR THE NIT

The electronic properties of CT salts are described by modified Hubbard models for mixed 1D stacks and electrostatic interaction within stacks or between stacks.[5–7,14,21,22,41] The neutral phase has N spin-paired electrons on $N/2$ donor sites. Following SSH,[40] the coupling between electrons and lattice phonons describes a harmonic lattice with a linear dependence of the hopping integral on the intersite distances[7,9,21] Similarly, linear coupling to molecular vibrations (e-mv) has been described in terms of a Holstein model with dispersionless harmonic molecular vibrations that modulate the site energies.[10,22,23] Coulomb interactions within chains are sometimes treated exactly,[11,15,22,23] but are more often included in a MF approximation for the 3D crystal.[5,10]

We take a modified Hubbard model with alternating on-site energies Γ, nearest-neighbor electron hopping t, and intersite electrostatic interactions V_{ij}. Since we are interested in structural instabilities, we just introduce coupling to zone-center phonons. The phonon δ drives the dimerization of the lattice, while the molecular vibration q describes the relaxation of the molecules as the on-site charge or ionicity ρ is varied. By setting the hopping integral of the regular chain as the energy unit, $t=1$, the general adiabatic Hamiltonian for a single chain with dimerization amplitude δ is

$$H_{CT} = (\Gamma + q)\sum_i (-1)^i \hat{n}_i - \sum_i [1 + (-1)^i \delta](c^{\dagger}_{i,\sigma} c_{i+1,\sigma} + \text{H.c.}) + \sum_{i,j}^{(3D)} V_{ij}\hat{\rho}_i\hat{\rho}_j + N\frac{q^2}{2\epsilon_{sp}} + N\frac{\delta^2}{2\epsilon_d}, \quad (1)$$

where the $\hat{\rho}_i$ operator is $\hat{\rho}_i = \hat{n}_i$ at even (A) sites and $\hat{\rho}_i = 2 - \hat{n}_i$ at odd (D) sites. Its expectation value ρ is independent of i and measures the degree of CT in the g.s.—i.e., the average on-site ionicity. Linear coupling to the adiabatic phonons δ and q is introduced, with the coupling strength measured by the relaxation energies ϵ_d and ϵ_{sp}, respectively. Both coordinates are harmonic, and the last two terms of H_{CT} describe the relevant potential energies. $2\Gamma = I - A$ measures the energy to transfer an electron from D to A, with I being the ionization potential of D and A the electron affinity of A. Γ implicitly includes U, the repulsion for setting two electrons on the same site.[5,41] In particular, the above Hamiltonian represents the $U \to \infty$ limit of the modified Hubbard model, where doubly ionized D^{++} or A^{--} sites are excluded on physical grounds.[5]

H_{CT} has been extensively investigated for $V_{ij}=0$: for small or vanishing ϵ_{sp} it has a continuous (second-order) dimerization instability that occurs far on the neutral side for large ϵ_d and moves towards intermediate ionicity for smaller ϵ_d.[9,22] The ionic lattice with $\Gamma < -0.666$ ($\rho > 0.686$) is unconditionally unstable toward dimerization.[9,22,42] Coupling to molecular vibrations qualitatively changes the picture: for large ϵ_{sp} a discontinuous (first-order) charge instability (NIT) sets in, with an abrupt increase of ρ as the system is driven from the neutral (N) to the ionic (I) state by tuning Γ.[7,22,43]

Three-dimensional electrostatic interactions are important, however, since the Madelung energy drives the NIT.[44] Electrons are delocalized along the stack, and i runs just on sites within one stack, but the sum over j in the third term of H_{CT} is actually over the crystal. As discussed elsewhere, the MF approximation for V-like interactions leads to reliable results when compared with exact diagonalization of stacks with V_{ij} restricted to 1D.[10–12] In the following we use the MF

for intersite interactions, thereby factoring the problem into single stacks that can be attacked exactly.

V-like interactions are conveniently split into two parts.[5] The first term $\Sigma_{i,odd} V\hat{\rho}_i\hat{\rho}_{i+1}$, where V is the intrachain nearest-neighbor interaction, is efficiently dealt with by a renormalization of $\Gamma \rightarrow \Gamma - V/2$: the energy required to ionize a DA pair (2Γ) is decreased by V due to nearest-neighbor interactions. A MF treatment of the remaining intersite interactions leads to

$$H_{MF} = \left(\Gamma - \frac{V}{2} + q - \epsilon_c\rho\right)\sum_i (-1)^i \hat{n}_i - \sum_i [1 + (-1)^i\delta](c^\dagger_{i,\sigma}c_{i+1,\sigma} + \text{H.c.}) + \frac{N}{2}\epsilon_c\rho^2 - N\epsilon_c\rho + N\frac{q^2}{2\epsilon_{sp}} + N\frac{\delta^2}{2\epsilon_d}, \quad (2)$$

where $\epsilon_c = V(\alpha - 1)$ and $V\alpha = \Sigma_j V_{ij}$ measures the Madelung constant. The first two lines of H_{MF} reduce to the standard modified Hubbard Hamiltonian with infinite U. It is defined in terms of just two parameters: $\Gamma_{eff} = \Gamma - \frac{V}{2} + q - \epsilon_c\rho$ and δ. This Hamiltonian can be readily diagonalized on the reduced valence bond (VB) basis for finite N to find the lowest eigenstate as a function of Γ_{eff} and δ. The resulting expectation value of ρ then allows for a self-consistent MF solution and gives, for fixed model parameters (Γ, α, ϵ_c, ϵ_{sp}, and ϵ_d), the total energy (per site) as a function of the vibrational coordinates, $\mathcal{E}(q,\delta)$. This function represents the adiabatic PES whose minima locate the equilibrium geometry for the given model.

Although simple, the model supports a fairly complex physics and catches the main features of the phase diagram of mixed-stack CT salts. Reliable estimates are available of some parameters of H_{MF}.[23] Taking the hopping integral $t \sim 0.21$ eV as the energy unit, current estimates for the strength of *e*-mv and *e*-ph coupling are $\epsilon_{sp} \sim 1.8$ and $\epsilon_d = 0.2-0.3$.[22,23] The Madelung constant is in the range $\alpha \sim 1-1.5$.[45] More delicate are estimates of V, the nearest-neighbor electrostatic interaction or, in the MF view, the factor that measures the global strength of the Madelung energy ($\epsilon_c \propto V$). Quantum chemical results set $V > 10t$,[45] but they completely neglect dielectric screening. Direct estimates of Γ also seem to be too large.[45] Here we discuss systems with fixed ϵ_{sp}, ϵ_d, and α. The neutral-ionic transition will be induced by increasing V, which mimics the reduction of the crystal's volume with decreasing temperature or increasing pressure. V is taken as adjustable, fixed at the value that best reproduces experiment.

Figure 1 shows results obtained for a system with a discontinuous NIT similar to that observed for TTF-CA. For each V, we search for the equilibrium states (minima in the PES) and plot their dimerization amplitude and ionicity. The discontinuity appears clearly, with ρ that smoothly increases from $\sim 0.2-0.3$ up to ~ 0.4 and then abruptly jumps towards the ionic limit $\rho \sim 0.6-0.7$. The stack stays regular ($\delta = 0$) on the N side and shows a finite dimerization ($\delta \sim 0.12$) in the I regime. The dotted vertical lines mark the region of multistability—i.e., the region where different nonequivalent

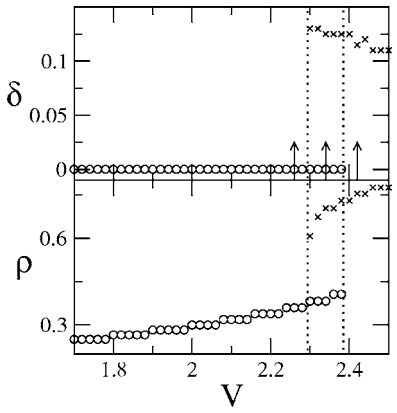

FIG. 1. The case of a discontinuous dimerization transition, with $\epsilon_d = 0.28$, $\epsilon_{sp} = 1.8$, $\alpha = 1.4$, and $\Gamma = 0.5$ in H_{MF}, Eq. (2). Results shown for $N = 16$ sites are similar to $N = 14$, not shown. The upper panel shows the dimerization amplitude δ; the lower panel is the ionicity ρ; dotted vertical lines mark the range of multistability; for clarity, the two phases are shown with different symbols. Arrows in the top panel mark the V values for which PES are drawn in Fig. 2

minima are found in the g.s. PES. Bistability is a typical feature of discontinuous phase transitions; the NIT shows tristability, however, since there are two equivalent ionic dimerized phases with equal and opposite δ.

Figure 2 shows the g.s. energy per site, $\mathcal{E}(q,\delta)$, as a function of the two vibrational coordinates q and δ calculated for the system described in Fig. 1 at three different V values (marked by arrows in the top panel of Fig. 1). The PES in the top panel of Fig. 2 ($V = 2.26$) is representative of a stable neutral (N) system with a single minimum. The PES in the bottom panel ($V = 2.42$) is instead characteristic of an ionic (I) stack, which, unconditionally unstable to dimerization, develops two equivalent minima at $\pm\delta$. The central panel of Fig. 2 ($V = 2.34$) shows multistability: three minima appear in the PES, one of them at $\delta = 0$ relevant to the regular N phase and two at $\pm\delta$ relevant to the dimerized I phase.

We can modify the nature of the phase transition by slightly changing the parameters of the electronic Hamiltonian while keeping the phonon model fixed. Just as an example, Fig. 3 shows the equilibrium ionicity and dimerization amplitude for a system with exactly the same parameters as in Fig. 1, but a smaller $\alpha = 1.1$. The transition is now continuous and amounts to a Peierls dimerization accompanied by a smooth increase of ρ from ~ 0.3 to ~ 0.75. There is, of course, no multistability for a continuous (second-order) transition. The PES evolves smoothly from a single minimum in the N phase to double minima in the I phase. The PES in Fig. 4 is drawn for $V = 2.94$, just at the border.

The systems in Figs. 2 and 4 are close to a charge and lattice instability—i.e., are located in a region of strong effective electron-vibration coupling, as shown by the softening of relevant frequencies and by the largely anharmonic PES. Both of these effects are driven by the electronic system, since the δ and q potentials in H_{MF} are manifestly harmonic. Softening and anharmonicity are obvious signatures of second-order transitions, but are usually not observed in discontinuous transitions. The NIT, however, is governed by a competition between a discontinuous crossover coupled to

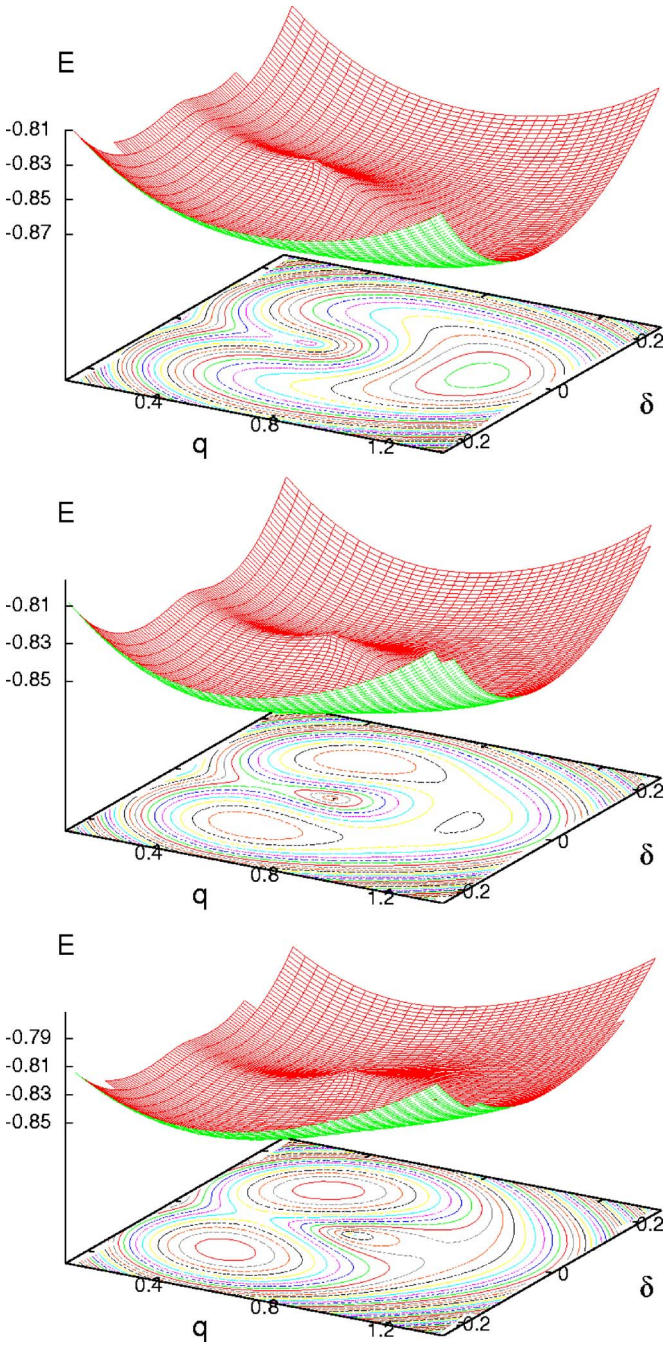

FIG. 2. (Color online) The PESs relevant to the system in Fig. 1. From top to bottom, $V=2.26$, 2.34, and 2.42.

on-site vibrations and a continuous dimerization transition driven by lattice phonons. When moving from the N to the I phase, a soft mode develops in any case, but in systems with large enough ϵ_c and/or ϵ_{sp} a discontinuous NIT with a condensation of q phonons takes place before the complete softening of the Peierls mode.

The q and δ coordinates entering the Hamiltonian in Eq. (1) are harmonic and mutually decoupled. Their interaction with the highly polarizable electrons delocalized along the stack makes the vibrations largely anharmonic and is also responsible for a mixing between the two coordinates,[27] as best recognized in the banana-shaped minima in the PES in

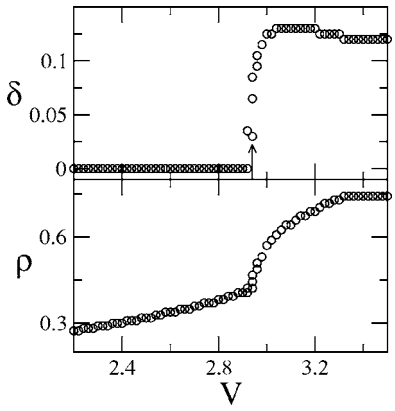

FIG. 3. The case of a continuous (Peierls) dimerization transition, with the same parameters as in Fig. 1 except for $\alpha=1.1$ instead of 1.4. Results shown for $N=16$ sites are similar to $N=14$, not shown. The arrow in the upper panel marks the V value for the PES in Fig. 4.

Fig. 4. Experimental evidence of soft lattice modes and of anharmonic coupling between lattice and molecular vibrations has been recently recognized by a detailed analysis of combination bands in TTF-CA and other salts.[28,46]

For the parameters in Fig. 1, the energy difference between the two stable phases is ~ 15 cm^{-1} (on a per-site basis) at the edges of the multistable region. Such small energy suggests that finite domains of the metastable phase can coexist at high temperature with the stable phase in systems with a discontinuous transition. The pressure-induced NIT of TTF-CA at ambient temperature is an example.[35,47,48] However, the energy to create a metastable domain has two contributions: in addition to the energy difference between stable and metastable phases, one has to consider the energy of the two boundaries. Whereas the first contribution is easily evaluated within models with correlation, much longer chains are needed to estimate boundary energies. In Sec. III we discuss a spinless fermion model for the NIT in order to find the energy and relaxation of domain walls.

III. METASTABLE DOMAINS OF SPINLESS FERMIONS

One-dimensional models of CT salts refer to the highest occupied molecular orbital (HOMO) of D and lowest unoc-

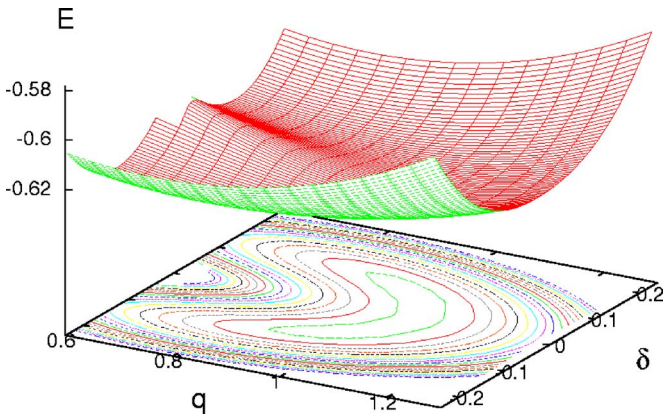

FIG. 4. (Color online) The PES relevant to the system in Fig. 3 with $V=2.94$.

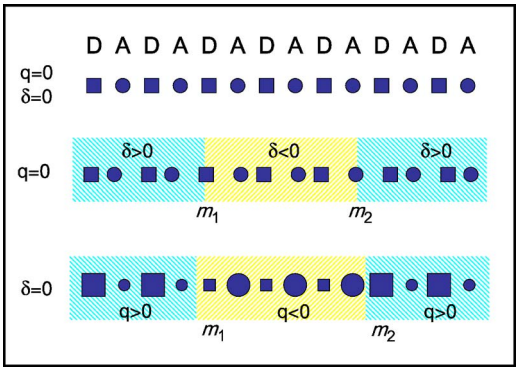

FIG. 5. (Color online) Schematic representation of a 1D mixed stack with D represented as squares and A as circles. The $q=\delta=0$ array has regular spacing and inversion centers at D and A. The dimerized array with $\delta>0$ and $q=0$ has degenerate gs with solitonic domain walls at m_1 and m_2. Coupling to molecular vibrations gives the $q>0$ array with $\delta=0$, a charge-density-wave (CDW) g.s. and CDW domain walls at m_1-1, m_1, and m_2-1, m_2. The shaded areas correspond to different domains.

cupied molecular orbital (LUMO) of A, while 1D models of conjugated polymers deal with carbon $2p_z$ atomic orbitals that yield wider bands by an order of magnitude. The SSH model[40] for polyacetylene illustrates topological solitons, or domain walls, between regions of opposite dimerization. The general Hamiltonian H_{CT} [Eq. (1)] reduces to the SSH model on setting $\Gamma=\epsilon_{sp}=V=q=0$. Coupling to the lattice phonon δ drives a Peierls instability and leads to the topological solitons shown in the middle line of Fig. 5 between regions with identical ρ and opposite dimerization, either $(DA)_n$ or $(AD)_n$.[49] Such domains are bond-order waves (BOWs). Coupling to the molecular vibration q leads instead to CDWs and domains with different ρ as shown schematically in the bottom line of Fig. 5. CDW domain walls are discussed below. They are similar to SSH solitons in some ways and quite different in other ways.

Domain walls can be treated quantitatively in a model with linear coupling of electrons to both δ and q, but without e-e correlation. We omit the spin degrees of freedom and all V_{ij} interactions in H_{CT}. With these approximations, the Hamiltonian is

$$H_0(\Gamma,\epsilon_{sp},\epsilon_d)=(\Gamma+q)\sum_p(-1)^p\hat{n}_p-\sum_p[1+(-1)^p\delta](a_p^\dagger a_{p+1}+\text{H.c.})+\frac{Nq^2}{2\epsilon_{sp}}+\frac{N\delta^2}{2\epsilon_d}. \quad (3)$$

H_0 describes a band of $N/2$ spinless fermions on N molecular sites with alternating site energy $\pm\Gamma$. The fermions occupy D sites (odd p) for $\Gamma\gg 0$ in the N stack and A sites for $\Gamma\ll 0$ in the I stack. The parameter Γ governs the NIT, and although V does not appear explicitly, it contributes to Γ_{eff} in Eq. (2) in the MF approximation.

The above Hamiltonian can be readily diagonalized for fixed q and δ (adiabatic approximation). The single-particle energies are

$$\epsilon_k=\pm\sqrt{(\Gamma+q)^2+4\cos^2 k+4\delta^2\sin^2 k}, \quad (4)$$

with $-\pi/2<k<\pi/2$ in the first Brillouin zone; the intermolecular spacing a, half the unit cell, is taken as 1. The valence band (negative ϵ_k) is filled in the g.s., while the conduction band (positive ϵ_k) is empty. The band gap is

$$E_g=2\sqrt{(\Gamma+q)^2+4\delta^2}. \quad (5)$$

The g.s. energy depends on three model parameters Γ, ϵ_d, and ϵ_{sp} as follows:

$$E_0(\Gamma,\epsilon_d,\epsilon_{sp})=-\frac{1}{N}\sum_{k=-\pi/2}^{\pi/2}\epsilon_k+\frac{\delta^2}{2\epsilon_d}+\frac{q^2}{2\epsilon_{sp}}. \quad (6)$$

For large N the sum becomes a complete elliptic integral of the second kind.[50] When drawn against q and δ, $E_0(\Gamma,\epsilon_d,\epsilon_{sp})$ gives the PES for spinless fermions: the minima of E_0 in the q-δ plane for fixed model parameters locate the equilibrium geometry of the lattice.

The equilibrium positions for the two vibrational coordinates are related to the CDW and BOW amplitudes ρ and β as follows:

$$q_{eq}=\epsilon_{sp}\left(\frac{1}{2}-\rho\right), \quad (7)$$

$$\delta_{eq}=\epsilon_d\beta, \quad (8)$$

where β, the BOW amplitude, measures the bond-order alternation and ρ is the g.s. expectation value of the ionicity operator, $\hat{\rho}=1/2+\Sigma_p(-1)^p n_p/N$, related to the site-CDW amplitude. It ranges from 0 to 1 much as in the correlated model in Sec. II. The general expressions for ρ and β are

$$\rho=\frac{1}{2}-\frac{1}{N}\sum_k\frac{\Gamma+q}{\sqrt{(\Gamma+q)^2+4\cos^2 k+4\delta^2\sin^2 k}}, \quad (9)$$

$$\beta=\frac{4}{N}\sum_k\frac{\delta\sin^2 k}{\sqrt{(\Gamma+q)^2+4\cos^2 k+4\delta^2\sin^2 k}}, \quad (10)$$

and can be evaluated for large N in terms of complete elliptic integrals.[50]

Aside from a spin factor, the SSH model corresponds to H_0 with $\Gamma=\epsilon_{sp}=0$. The degenerate g.s. is a BOW with dimerization $\pm\delta$ for $\epsilon_d>0$, and the band gap is 4δ. Solitons mark dimerization reversals as shown in the middle line of Fig. 5. Rice and Mele[51] found solitons for $\Gamma>0$ and $\epsilon_{sp}=0$ in H_0; dimerization is now conditional and restricted to Γ smaller than a critical value that depends on ϵ_d. BOW ground states with $\pm\delta$ are always degenerate. Kivelson extended the SSH model to coupling to a molecular vibration, or $\epsilon_{sp}>0$ in our notation, while retaining equal site energies ($\Gamma=0$).[52] He discussed the competition between a BOW favored by e-ph coupling and a CDW favored by e-mv coupling. The resulting phase diagram is the same for spinless fermions at $\Gamma=0$: aside from a very narrow region with strong e-ph and e-mv coupling where both instabilities are supported, the g.s. is either a BOW or a CDW.

Figure 6 shows $\rho(\Gamma)$ calculated for spinless fermions with $\delta=\epsilon_d=0$ and $\epsilon_{sp}=0,1.0,1.5$. The S-shaped $\rho(\Gamma)$ curves ob-

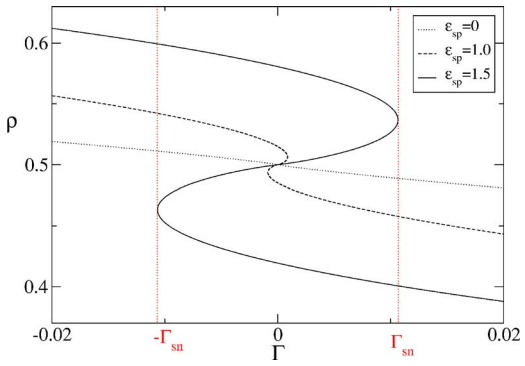

FIG. 6. (Color online) The ionicity ρ vs Γ calculated for three values of ϵ_{sp}. The spinodals $\pm\Gamma_{sn}$ mark the bistable region for $\epsilon_{sp}=1.5$.

tained for finite ϵ_{sp} signal CDW formation and multistable behavior: for a specific Γ in the multistable region, two stable states correspond to the two points on the $\rho(\Gamma)$ curve with negative slope and an unstable state corresponds to the point with positive slope. The charge instability of H_0 is unconditional at $\Gamma=0$, since Eq. (7) has solution with finite q_{eq} for any $\epsilon_{sp}>0$. In other terms, the g.s. PES has three extrema for $\epsilon_{sp}>0$ at $\Gamma=0$. The state with $\rho=0.5$ is a maximum; the other two are equivalent minima at $\pm q_{eq}$ [cf. Eq. (8)], with ρ symmetrically located about 0.5. Since the degenerate CDWs at $\Gamma=0$ are interchanged on changing the sign of q_{eq}, sharp domain walls correspond to successive site energies $-q_{eq}$, $-q_{eq}$ or q_{eq}, q_{eq} along the stack.

The band gap E_g in Eq. (5) sets the energy scale in units of t, which is 2–3 eV in conjugated polymers[40] and 0.1–0.3 eV in CT salts.[53] The SSH gap of 4δ is due to dimerization, while the CDW gap of $2q_{eq}$ at $\Gamma=0$ is due to molecular relaxation along q. Each SSH soliton generates a localized state in the gap. The energy of two sharp or relaxed solitons is E_g or $\sim 2E_g/\pi$, respectively. Sharp CDW reversals at $\Gamma=0$ involve four sites and generate four localized states, two at each wall, which can be found analytically by constructing a bonding and antibonding linear combination of two Wannier functions at each wall. When the walls are far apart, the localized MOs derived from the valence band are centered at the $-q_{eq}$, $-q_{eq}$ wall and have energy

$$\epsilon_{loc} = -\sqrt{1+q_{eq}^2} \pm 1. \tag{11}$$

The lower ϵ_{loc} is below the band edge at $\epsilon_0=-\sqrt{q_{eq}^2+4}$. The HOMO is the higher ϵ_{loc} and is a gap state, above the band edge at $\epsilon_{\pm\pi/2}=-q_{eq}$. Localized states derived from the conduction band are centered at the q_{eq}, q_{eq} wall and have energy $-\epsilon_{loc}$. The LUMO is a localized gap state. For small $q_{eq}<1$, the energy of two domain walls at $\Gamma=0$ can be estimated by transferring two spinless fermions at band edges to ϵ_{loc},

$$2E_w(0) = -2\sqrt{1+q_{eq}^2} + q_{eq} + \sqrt{4+q_{eq}^2} \sim q_{eq} - \frac{3}{4}q_{eq}^2. \tag{12}$$

We note that $2E_w(0)<E_g/2$ is less than half the energy of two SSH solitons. This difference makes domain walls thermally accessible even at $k_BT<E_g$, where thermal excitation across the gap is negligible.

At finite but not too large Γ, bistable solutions are found (cf. Fig. 6), but the two stable states are no longer degenerate and their ρ are no longer symmetrically located around 0.5. The stable phase (lower-energy minimum) and the metastable phase (higher-energy minimum) then correspond to two different equilibrium q values, which, for the sake of clarity, will be referred to as c and c', respectively. Again the two phases may be interchanged by a mismatch in the on-site distortion. At variance with the $\Gamma=0$ case, the energy required to create a metastable domain in the stable lattice linearly increases with the length of long enough domains. This resembles the coexistence of N domains in an I lattice (or vice versa) that was suggested in Sec. II for the correlated model in the multistable regime.

To discuss relaxed boundaries, we have to describe local vibrational modes, which are taken as dispersionless for molecular vibrations. The site energy entering Eq. (3) is then locally modulated as $(\Gamma+q_p)$, and the potential energy becomes $\Sigma_p q_p^2/2\epsilon_{sp}$, where q_p is the coordinate that describes the local vibration on site p; notice that $q=\Sigma_p(-1)^p q_p/\sqrt{N}$ is the zone-center coordinate of the diatomic lattice (finite Γ and/or finite δ, unit cell $2a$). The electronic problem at fixed geometry can be solved numerically on finite-size systems with large N by imposing cyclic boundary conditions and either sharp or relaxed domain walls. We consider a metastable CDW domain that starts at sites $p=m_1$ and ends at $p=m_2-1$, with m_1 and m_2 even by definition. Again following SSH ideas,[40] we study relaxation in terms of variable half widths ξ_1 and ξ_2, so that q_p is defined as follows:

$$q_p = c + \frac{c'-c}{2}\tanh\frac{p-m_1+0.5}{\xi_2} - \frac{c'-c}{2}\tanh\frac{p-m_2+0.5}{\xi_2}, \quad p<m_1,\ p\geqslant m_2,$$

$$q_p = c + \frac{c'-c}{2}\tanh\frac{p-m_1+0.5}{\xi_1} - \frac{c'-c}{2}\tanh\frac{p-m_2+0.5}{\xi_1}, \quad m_1\leqslant p\leqslant m_2-1. \tag{13}$$

We have $\xi_1=\xi_2$ in the degenerate case when $\Gamma=0$ and equal relaxation on either side of domain walls with width 2ξ. Relaxation is governed by ξ_2 in the stable phase and by ξ_1 in the metastable phase for $\Gamma>0$. Sharp domain walls have $\xi_1\sim\xi_2<1$. The envelope functions in Eqs. (13) come from continuum models and reduce the relaxation problem to finding ξ_1 and ξ_2, which minimize the total energy.

For $\Gamma=0$ and finite ϵ_{sp}, the q_p in Eqs. (13) describe a domain of length $L=m_2-m_1$ of one of the two degenerate phases embedded into a chain of the other phase (cf. Fig. 5). The relevant energy is shown in Fig. 7 as a function of L for a chain with $\Gamma=0$, $\epsilon_{sp}=1.5$, and different $\xi=\xi_1=\xi_2$ values. Since the two stable phases are degenerate, the energy is just that of two domain walls. The energy of sharp domain

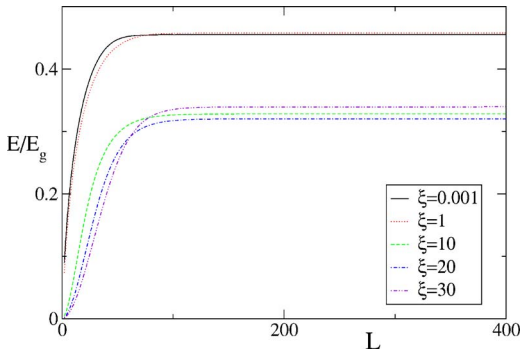

FIG. 7. (Color online) The energy (in units of the gap) of an $N=600$ site chain with $\Gamma=0$ and $\epsilon_{sp}=1.5$: the two degenerate phases are exchanged at m_1 and m_2 so that a domain of length $L=m_2-m_1$ is created.

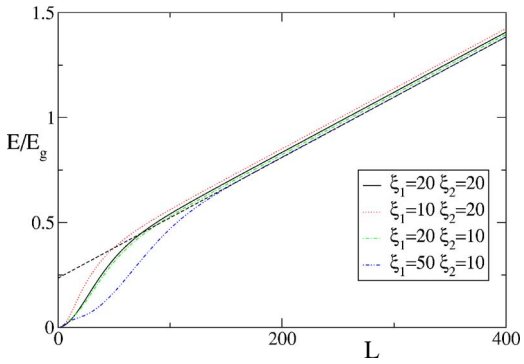

FIG. 8. (Color online) The energy (in units of the gap) of an $N=600$ site chain with $\Gamma=0.005$ and $\epsilon_{sp}=1.5$ when a metastable domain of length $L=m_2-m_1$ is created.

walls with $\xi=0.001$ saturate for $L>50$. Direct solution at $\epsilon_{sp}=1.5$ agrees with $2E_w(0)$ in Eq. (12) to three digits. A width of $\xi\sim 20$ lattice constants is optimal and lowers $2E_w(0)$ by $\sim 30\%$, an amount that is quite similar to the SSH relaxation. The energy of the domains becomes independent of their separation for $L>100$. Direct solution at $\Gamma=0$ also confirms quantitatively the presence of localized states and their energies discussed above.

Any $\epsilon_{sp}>0$ breaks the symmetry of the chain at $\Gamma=0$, leading to two degenerate phases $\pm q_{eq}$. The $\Delta\rho$ discontinuity becomes, however, exponentially small for small $\epsilon_{sp}<1$. At finite Γ the symmetry breaking becomes conditional, and for any ϵ_{sp} spinodals mark the boundary of multistability regions. Figure 6 explicitly shows the spinodals at $\Gamma_{sp}=0.01065$ as obtained for $\epsilon_{sp}=1.5$. The g.s. and metastable phase for $\Gamma>0$ have $\rho<1/2$ and $>1/2$, respectively. Small $\Delta\rho<0.2$ gives a narrow range of metastability, a conclusion that also follows for correlated systems described by H_{CT}.

The choice of $\Gamma=0.005$ is within the metastable regime for $\epsilon_{sp}=1.5$. A large metastable domain of length L has energy

$$E(L,\Gamma)=2E_w(\Gamma)+L\Delta E_0(\Gamma). \tag{14}$$

The first term accounts for the energy of the two domains walls of the kind shown in Fig. 5 whose relaxation we consider below. The L-dependent second term goes as the energy difference per site, $\Delta E_0(\Gamma)$, between the metastable and stable phases. This contribution is independent of the domain relaxation and dominates at large L. Figure 8 shows $E(L)/E_g$ vs L for $\Gamma=0.005$, $\epsilon_{sp}=1.5$, and $\epsilon_d=0$. The g.s. has $c=0.140$, which leads to $E_g=0.280$ and $\rho=0.41$. In accordance with Eq. (14), all the curves in Fig. 8 have equal slopes for $L>100$. The lowest $E(L)$ for well-separated domain walls occurs around $\xi_1\sim 50$ and $\xi_2\sim 10$ in Eq. (13). The dashed straight line is $L\Delta E_0(\Gamma)$ and shows that $2E_w$ is half as large at $\Gamma=0.005$ as at $\Gamma=0$. Results at $\Gamma=0.01$ yield even smaller $2E_w$.

We conclude that the energy of metastable domains of $L>100$ is mainly due to the second term of $E(L,\Gamma)$. Moreover, Taylor expansion of $\Delta E_0(\Gamma)$ about $\Gamma=\Gamma_c$, where the energies are equal, gives

$$\Delta E_0(\Gamma)=(\Gamma-\Gamma_c)\Delta\rho(\Gamma_c)+o(\Gamma-\Gamma_c)^2. \tag{15}$$

This relation follows from the Hellmann-Feymann theorem and holds for correlated models such as H_{CT} with a first-order transition at Γ_c, which may also involve dimerization. The slope of $E(L)$ in Fig. 8 is accurately given by $\Delta\rho$ at $\Gamma_c=0$, and this result has been explicitly confirmed for other Γ values in the bistability region. Solution of H_0 is straightforward up to $N\sim 1000$ sites and yields quantitative information about metastable domains of spinless fermions.

Soliton relaxation in the SSH model modulates the transfer integrals near dimerization reversals. Such modulation does not alter the charge distribution of the half-filled band, however, which is fixed at precisely one electron per site by electron-hole (e-h) symmetry. H_0 has e-h symmetry in the special case of $\Gamma=\epsilon_{sp}=q=0$ in Eq. (3), but site energies and/or e-mv coupling break e-h symmetry. Figure 9 shows the ionicity at CDW crossovers of H_0 with $\epsilon_{sp}=1.5$ in domains of $L=300$ sites. The top panel has $\Gamma=0$ and degenerate phases with $\rho=0.419$ and 0.581. Sharp domain walls generate rapid oscillations of ρ around sites $m_1=100$ and $m_2=400$. The oscillations are strongly damped in the relaxed walls with $\xi=20$, which minimizes $2E_w(0)$ in Fig. 7 and broadens the crossover region. The lower panel of Fig. 9 shows a relaxed metastable domain of $L=300$ with the same parameters except for $\Gamma=0.005$. The stable and metastable phases now have $\rho=0.410$ and 0.570, respectively. Oscillations in ρ persist in relaxed walls whose widths minimize the energy in Fig. 8 and extend well into the metastable domain. As expected on general grounds, domains of $L>\xi_1+\xi_2\sim 60$ are needed to have independent walls and constant ρ within domains. But constant ρ is unnecessarily stringent at the present resolution of ionicity; a domain of $L\sim 100$ in the lower panel of Fig. 9 would still have $\rho>0.5$, which can be distinguished from the $\rho=0.4$ of the stable phase.

IV. PRESSURE-INDUCED TRANSITION OF TTF-CA

In this section we model TTF-CA. The parameters in Figs. 1 and 2 were previously used for the 81-K transition on cooling.[10,23] There is a $\Delta\rho$ jump of $\sim 0.2-0.3$,[31] evidence for coexisting phases over $\sim 2-3$ K,[54] and a well-characterized

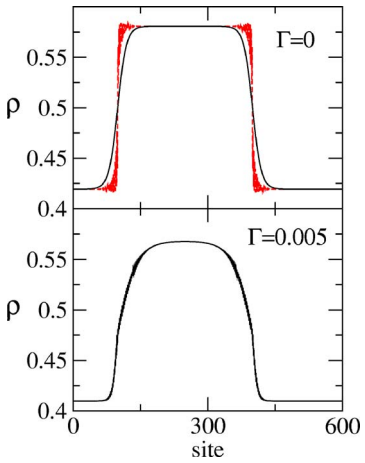

FIG. 9. (Color online) The on-site charge of an $N=600$ site chain with domain walls located at $m_1=100$ and $m_2=400$. Top panel: $\Gamma=0$ and $\epsilon_{sp}=1.5$, the two curve show results for $\xi=0.001$ and 20. Bottom panel: $\Gamma=0.00$ and $\epsilon_{sp}=1.5$, $\xi_1=50$ and $\xi_2=10$.

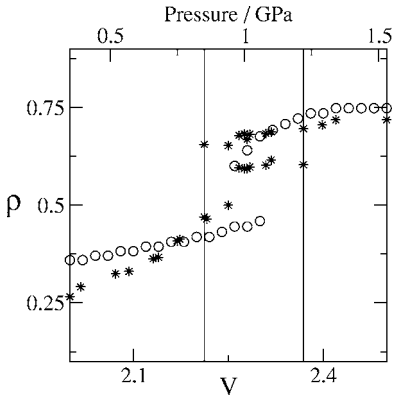

FIG. 10. The pressure-induced NIT of TTF-CA at ambient temperature. Stars report experimental $\rho(P)$ data (from Ref. 35); vertical lines mark the corresponding bistability range. Circles show calculated $\rho(V)$ for a 16-site chain with $\epsilon_d=0.2$, $\epsilon_{sp}=1.6$, $\alpha=1.3$, and $\Gamma=0.4$ in H_{MF}, Eq. (2). A linear relation between the P and V scales (top and bottom x axes) is assumed in the proximity of $V_c=P_c$.

3D structural change.[55] There is no structural data for the pressure-induced transition at 300 K whose vibrational analysis in single crystals has recently been presented.[35,56] The frequency of the $b_u\nu_{10}$ mode of CA in the midinfrared decreases by 160 cm^{-1} between $\rho=0$ and 1 in reference compounds.[35,56] Under properly defined conditions, the ionicity of CT salts is based on the measured frequency of ν_{10} assuming a linear dependence on ρ.[30] The left panel of Fig. 2 in Ref. 35 shows ρ as a function of pressure at 300 K, as estimated from vibrational data. Two IR peaks are resolved between 0.86 and 1.22 GPa in the frequency region of ν_{10}. The relative intensity of the two peaks reaches 50% between 1.0 and 1.1 GPa.[35,56] We then locate the critical pressure $P_c\sim 1.04$ GPa and interpret the two-peak region in terms of metastable domains set by spinodals at 0.86 and 1.22 GPa.

Compared with the 81-K transition, the pressure-induced transition has smaller $\Delta\rho\sim 0.07$ and higher $\rho_N\sim 0.5$ at the onset. Smaller $\Delta\rho$ suggests smaller ϵ_{sp} while higher ρ_N indicates smaller ϵ_d. The electronic system is less strongly coupled to either molecular vibrations or lattice phonons. A qualitative explanation is that t, the unit of energy, depends on the intermolecular overlap and is consequently more sensitive to volume changes than are electrostatic interactions. Increasing P clearly increases t, and increasing t is known to suppress the $\Delta\rho$ discontinuity.[5,7,11,22] Under cooling, by contrast, volume changes increase t while reduced thermal motions reduce t.

The 81-K transition in Figs. 1 and 2 is modeled with $\epsilon_{sp}=1.8$ leading to $\Delta\rho\sim 0.3$ and with $\epsilon_d=0.28$ leading to maximum dimerization $\delta=0.12$. The pressure-induced transition can be modeled in terms of a larger t and hence of smaller Γ, α, ϵ_{sp}, and ϵ_d, as shown in Fig. 10, for parameters chosen to have $\rho\sim 0.5$ at the transition and an ionicity jump consistent with the experimental data. Although the Coulomb interaction V is expected to increase with pressure, the function $P(V)$ is neither known nor linear. Nevertheless, there must be a linear regime around V_c or P_c. Therefore in Fig. 10 we superimpose experimental $\rho(P)$ data from Ref. 35 (stars, P on the top x axis) and calculated $\rho(V)$ results (open circles, V on the bottom x axis). The vertical lines mark the observed range of bistability. This preliminary modeling is qualitative. In fact, not only a nonlinear $V(P)$ dependence is expected, but finite-size effects become important near the metallic point that the system approaches when ϵ_{sp} and ϵ_d are small. Comparison of $N=16$ and 14 results indicates good convergence except in the immediate vicinity of V_c where ρ varies the most rapidly. Larger N and extrapolations are needed at weakly first-order transitions even at the MF level. Moreover, the PES at such transitions has shallow minima whose analysis poses separate numerical challenges.

The next question is the thermal population of metastable domains. On general grounds, small $\Delta\rho$ implies a narrow range of multistability. Thermal excitation requires $k_BT\sim E(L,\Gamma)$, where $E(L,\Gamma)$ in Eq. (14) is the excitation energy of a domain of length L. Vibrational data (cf. Fig. 1 of Ref. 35) suggest that the fraction of I domains increases smoothly from $\sim 5\%$ $\sim e^{-2}$ at the onset of bistability to $\sim 95\%$ at the end of bistability. The intensity of the two infrared bands assigned to the ν_{10} mode of CA molecules with different ρ's varies smoothly, strongly suggesting a simple equilibrium between two phases that are degenerate at $P_c=1.04$ GPa. The relative intensities indicate that $E(L,\Gamma)$ is about $2k_BT$ for metastable I domains at $P=0.86$ GPa or for metastable N domains at $P=1.22$ GPa. It follows that $4k_BT$ sets a limit on the formation of thermally accessible metastable domains at the pressure-induced NIT. For correlated systems, we use Eq. (15) and the observed $\Delta\rho(\Gamma_c)$ for the excitation energy per site, $\Delta\epsilon_0(\Gamma)$. Neglecting temporarily the domain wall energy $2E_w(\Gamma)$, we find the minimum L,

$$L_{min}(\Delta\Gamma)_{ms}\Delta\rho(\Gamma_c)=4k_BT/t. \tag{16}$$

We have $t\sim 0.21$ eV (2300 K), which increases under pressure, so that the right-hand side of the above equation is $\sim 1/2$ at 300 K. The observed $\Delta\rho\sim 0.07$ and estimated $(\Delta\Gamma)_{ms}\sim 0.07$ for either spinless fermions or correlated systems leads to $L_{min}\sim 100$ at the pressure-induced transition.

The same estimate at the 81-K transition returns $L_{min}<10$ when larger $\Delta\rho$ and $(\Delta\Gamma)_{ms}$ are taken into account. These L_{min} are upper bounds because $2E_w(\Gamma)$ has been neglected.

Neutral-ionic domain walls (NIDWs) are the elementary excitations at the transition.[21,32] $2E_w(0)$ in Eq. (12) is the quantitative result for spinless fermions and small $\pm q_{eq}$. Since we have $\Delta q_{eq}=\epsilon_{sp}\Delta\rho(\Gamma_c)$ at the transition for either spinless fermions or correlated systems, we estimate that $2E_w(0)\sim t\epsilon_{sp}\Delta\rho/2$. Then $\epsilon_{sp}\sim 1.6$ at the pressure-induced transition leads to $2E_w(0)\sim 130$ K. Our estimate is more quantitative and completely independent of Nagaosa's conclusion[21] that NIDWs were thermally accessible in TTF-CA at 300 K. Larger $\epsilon_{sp}\sim 1.8$ and $\Delta\rho\sim 0.2-0.3$ at the 81-K transition lead to $2E_w(0)>500$ K. The concentration of domains walls in TTF-CA is small even at $T_c=81$ K, and the domain walls detected by spin resonance[57] at $T<T_c$ are associated with adventitious solitons.[49,57] Although the estimates of $2E_w(0)$ and L_{min} are approximate, the trends are clear: Metastable domains are thermally accessible at the pressure-induced transition but not at the 81-K transition. More generally, small $\Delta\rho$, as well as high T favors the formation of metastable domains.

V. DISCUSSION

Microscopic models such as the Peierls-Hubbard model H_{CT} in Eq. (1) have been widely applied to CT salts. Exact solutions are limited to finite N, and the PESs in Figs. 2 and 4 are based on $N=16$ sites. The comparison with $N=14$ results indicates minor finite-size effects, as also confirmed by exact results for the electronic model (H_{CT} with $\epsilon_d=\epsilon_{sp}=0$) up to $N=22$ sites, which indicate satisfactory convergence for the g.s energy per site for the ionicity and for excitation thresholds.[42] The PESs show the dependence of the g.s. energy on the two zone-center coordinates δ and q coupled to the electrons via the modulation of the BOW and CDW, respectively. In the N regime a single minimum PES at $\delta=0$ is found, whereas a symmetry-broken PES with two equivalent minima $\pm\delta$ is found in the I regime. The transition region is particularly interesting: the competition between the two phases, driven by the balance between Γ, the on-site energy alternation, and the Madelung energy, is delicate and is profoundly affected by e-ph coupling. Continuous (second-order) phase transitions can be observed where the smooth evolution of the g.s. PES from a single- to a double-minimum structure goes through a very interesting banana-shaped surface (Fig. 4). For different model parameters the transition becomes discontinuous: the crossover between the two phases goes through a region where three-minimum PESs are observed. One of the minima describes an N regular ($\delta=0$) phase that coexists with an ionic dimerized phase, described by the two equivalent minima at $\pm\delta$.

To relate the recent observation of coexisting phases in the pressure-induces NIT of TTF-CA[35,56] with the calculated multistability, estimates are needed of the energy of domain boundaries. Reliable modeling of boundary energies and relaxation requires calculations on much longer chains than affordable for correlated models. To such an aim we introduced a noninteracting spinless-fermion model for the NIT: In conjugated polymers, many aspects of uncorrelated SSH solitons carry over to correlated π-electron systems or to all-electron quantum chemical calculations.[40,58] There are also clear failures related to neglecting electron correlation, notably the energy of even-parity states. We are assuming that the exact results on metastable phases of the uncorrelated spinless fermion model give insight into correlated metastable domains of H_{CT}.

The critical behavior of $\rho(\Gamma)$ in Fig. 6 is typical for any first-order phase transition.[59] The phases are degenerate at Γ_c for H_{CT}, but in general the spinodals are not symmetric about Γ_c. The PESs in Fig. 2 illustrate tristable behavior with finite $\Delta\rho(\Gamma_c)$. The phase with smaller ρ is the g.s. of H_{CT} for $V<V_c$, while the dimerized ionic phase is metastable up to the spinodal. For $V>V_c$, the dimerized ionic phase is the g.s. and the regular neutral phase is metastable down to the spinodal. As in the case of spinless fermions, small $\Delta\rho(\Gamma_c)$ implies a narrow bistable region about Γ_c and governs the $E(L,\Gamma)$ of metastable domains in Eqs. (14) and (15).

Coexistence at the NIT was first discussed by Nagaosa[21,32] in terms of a model closely related to H_{CT} in Eq. (1). Specifically, Nagoasa took $\Delta=\Gamma$, large but finite U, which largely excludes D^{2+} and A^{2-} sites, and nearest-neighbor V along the stack, which we also adopt in Eq. (2). He also introduced $S=4\epsilon_d$ for coupling to lattice phonons, but disregarded coupling to molecular vibrations. Nagaosa's results were based on Monte Carlo simulations for stacks with $N=40$ at finite T. Our exact results at zero temperature are obtained for smaller N in correlated systems and much larger N for spinless fermions, and are relevant to a quantum or g.s. transition driven by volume changes.[20] Modeling electronic spectra, Nagaosa discussed coexistence in the proximity of a discontinuous NIT in terms of lattice-relaxed NIDWs LR-NIDWs.[21,32] He estimated their properties for the degenerate case in a phenomenological continuum model and found a small creation energy, of the order of 300 K for TTF-CA parameters.

We have discussed instead vibrational spectra that provide more detailed information about ρ. Spinless fermions in Sec. III yield detailed information about metastable domains and relaxed domain walls. Since the length dependence is related to the discontinuity of ρ in either uncorrelated or correlated models, we can set more stringent minimum requirements for the formation of metastable domains than obtained from the continuum model. As noted in Sec. III, CDW domain walls connect nondegenerate regions except at $\Gamma=0$ for spinless fermions or at $\Gamma=\Gamma_c$ in the correlated model. The width of CDW domains walls, $\xi_1+\xi_2$ in Eq. (13), is asymmetric in general and wider on the metastable side. The widths reported in Fig. 9 offer a strong evidence that the length of metastable domains must exceed $N\sim\xi_1+\xi_2>30$ lattice constants in order to resolve ρ_1 and ρ_2. Hence the present model does not support short domains.

LR-NIDW concepts have been widely applied to CT salts with mixed stacks. NIDWs have been invoked for nondegenerate phases[33,60–62] without, however, including the length-dependent energy of metastable domains. Short NIDWs of a few lattice constants are also problematic within the continuum model,[32] but have been suggested for TTF-CA.[33,60–62] The interpretation of such results is beyond the scope of the

present work. The main points here are (a) that metastable domains must be close to a first-order transition, (b) that $E(L,\Gamma)$ in Eq. (14) for the formation of a metastable domain depends mainly on its length, and (c) that a minimum length of $L\sim 30$ lattice constants is required for the definition of a domain.

The appearance of multistability near a discontinuous phase transition is expected, and a PES with three minima for such NIT systems has long been foreseen.[22,32] Of special interest is the $E(\delta)$ curve in Fig. 1 of Ref. 32, which has since been used to interpret a variety of data[33,34,60,63] and has also been related to the classical Blume-Emery-Griffiths model of an array of $S=1$ spins.[64] In another case, a three-minimum potential curve has been imposed by introducing largely anharmonic phonons.[65] A $E(\delta)$ curve with three minima can be viewed as the projection of $\mathcal{E}(q,\delta)$ in the middle panel of Fig. 2 onto the E-δ plane. In contrast to previous discussions, however, our PESs result from the adiabatic diagonalization of a microscopic model without any *ad hoc* assumption about intrinsically anharmonic phonons. Bare phonons entering our Hamiltonians are rigorously harmonic. Large anharmonicity emerges naturally from coupling harmonic phonons to delocalized electrons: the multistability of the PESs simply reflects the intrinsic instabilities of the electronic system.

The highly anharmonic PESs in Figs. 2 and 4 offer the clearest evidence for the amplification of e-ph coupling near an electronic instability. Moreover, the banana-shaped PES in Fig. 4 demonstrates strong q-δ coupling arising from linear coupling of both modes to the same, highly polarizable electronic system at the Peierls transition. Explicit consideration of slow nuclear degrees of freedom makes it possible to construct PESs for microscopic models of NIT systems that, although idealized in several respect, are realistic enough for comparison with diverse experiments. Organic CT salts with NITs are interesting examples of *soft electronic behavior*,[4] arising from the competition between ground states with site-or bond-density waves. Competing interactions lead to the rich physics of NIT systems which, nevertheless, are described approximately by a 1D modified Hubbard model with coupling to both lattice phonons and molecular vibrations. Such a microscopic model provides a good starting point for systems with coupled electronic and structural instabilities.

ACKNOWLEDGMENTS

A.P. thanks A. Brillante, G. D'Avino, R.G. Della Valle, A. Girlando, and M. Masino for useful discussions. Work in Parma was supported by Italian MIUR through Grant No. FIRB-RBNE01P4JF.

*Electronic address: soos@princeton.edu
†Electronic address: anna.painelli@unipr.it; http://continfo.chim.unipr.it/mmaa/

[1] J. E. Hirsch, Phys. Rev. Lett. **53**, 2327 (1984).
[2] J. Voit, Phys. Rev. B **45**, 4027 (1992).
[3] S.-J. Gu, S.-S. Deng, Y.-Q. Li, and H.-Q. Lin, Phys. Rev. Lett. **93**, 086402 (2004).
[4] E. Dagotto, Science **309**, 257 (2005).
[5] Z. G. Soos and S. Mazumdar, Phys. Rev. B **18**, 1991 (1978).
[6] N. Nagaosa and J.-I. Takimoto, J. Phys. Soc. Jpn. **55**, 2735 (1986).
[7] A. Girlando and A. Painelli, Phys. Rev. B **34**, 2131 (1986).
[8] R. Resta and S. Sorella, Phys. Rev. Lett. **82**, 370 (1999).
[9] L. DelFreo, A. Painelli, and Z. G. Soos, Phys. Rev. Lett. **89**, 027402 (2002).
[10] Z. G. Soos, S. A. Bewick, A. Peri, and A. Painelli, J. Chem. Phys. **120**, 6712 (2004).
[11] Z. G. Soos, S. Kuwajima, and R. Harding, J. Chem. Phys. **85**, 601 (1986).
[12] A. Painelli and F. Terenziani, J. Am. Chem. Soc. **125**, 5624 (2003).
[13] K. Iwano, Phys. Rev. Lett. **97**, 226404 (2006).
[14] N. Nagaosa and J.-I. Takimoto, J. Phys. Soc. Jpn. **55**, 2745 (1986).
[15] O. Legeza, K. Buchta, and J. Sólyom, Phys. Rev. B **73**, 165124 (2006).
[16] J. B. Torrance, A. Girlando, J. J. Mayerle, J. I. Crowley, V. Y. Lee, P. Batail, and S. J. LaPlaca, Phys. Rev. Lett. **47**, 1747 (1981).
[17] A. Girlando, A. Painelli, S. A. Bewick, and Z. G. Soos, Synth. Met. **141**, 129 (2004), and references therein.
[18] S. Horiuchi, R. Kumai, Y. Okimoto, and Y. Tokura, Chem. Phys. **325**, 78 (2006), and references therein.
[19] S. Horiuchi, Y. Okimoto, R. Kumai, and Y. Tokura, J. Am. Chem. Soc. **123**, 665 (2001).
[20] S. Horiuchi, Y. Okimoto, and Y. Tokura, Science **229**, 299 (2003).
[21] N. Nagaosa, J. Phys. Soc. Jpn. **55**, 2754 (1986).
[22] A. Painelli and A. Girlando, Phys. Rev. B **37**, 5748 (1988).
[23] A. Painelli and A. Girlando, J. Chem. Phys. **87**, 1705 (1987).
[24] S. Mazumdar and S. N. Dixit, Phys. Rev. Lett. **51**, 292 (1983).
[25] T. Egami, S. Ishihara, and M. Tachiki, Science **261**, 1307 (1993).
[26] A. Lanzara, P. V. Bogdanov, X. J. Zhou, S. A. Kellar, E. D. L. D. L. Feng, T. Yoshida, H. Eisaki, A. Fujimori, K. Kishio, J.-I. Shimoyama *et al.*, Nature (London) **412**, 510 (2001).
[27] A. Painelli and Z. G. Soos, Chem. Phys. **325**, 48 (2006).
[28] M. Masino, A. Girlando, and Z. G. Soos, Chem. Phys. Lett. **369**, 428 (2003).
[29] A. Girlando, R. Bozio, C. Pecile, and J. B. Torrance, Phys. Rev. B **26**, 2306 (1982).
[30] A. Painelli and A. Girlando, J. Chem. Phys. **84**, 5655 (1986).
[31] A. Girlando, F. Marzola, C. Pecile, and J. B. Torrance, J. Chem. Phys. **79**, 1075 (1983).
[32] N. Nagaosa, J. Phys. Soc. Jpn. **55**, 3488 (1986b).
[33] M. H. Lemee-Cailleau, M. LeCointe, H. Cailleau, T. Luty, F. Moussa, J. Roos, D. Brinkmann, B. Toudic, C. Ayache, and N. Karl, Phys. Rev. Lett. **79**, 1690 (1997).
[34] H. Sakamoto, K. Mizoguchi, and T. Hasegawa, Phys. Rev. Lett.

93, 186401 (2004).
[35] M. Masino, A. Girlando, A. Brillante, R. G. D. Valle, and E. Venuti, Mater. Sci. Poland **22**, 333 (2004).
[36] S. Horiuchi, T. Hasegawa, and Y. Tokura, J. Phys. Soc. Jpn. **75**, 051016 (2006), and references therein.
[37] T. Suzuki, T. Sakamaki, K. Tanimura, S. Koshihara, and Y. Tokura, Phys. Rev. B **60**, 6191 (1999).
[38] S. Iwai, Y. Ishige, S. Tanaka, Y. Okimoto, Y. Tokura, and H. Okamoto, Phys. Rev. Lett. **96**, 057403 (2006).
[39] M. Masino and A. Girlando (private communication).
[40] A. J. Heeger, S. Kivelson, J. R. Schrieffer, and W. P. Su, Rev. Mod. Phys. **60**, 781 (1988).
[41] P. J. Strebel and Z. G. Soos, J. Chem. Phys. **53**, 4077 (1970).
[42] Y. Anusooya-Pati, Z. G. Soos, and A. Painelli, Phys. Rev. B **63**, 205118 (2001).
[43] A. Painelli, L. D. Freo, and Z. G. Soos, Synth. Met. **133–134**, 619 (2003).
[44] H. M. McConnell, B. M. Hoffmann, and R. M. Metzger, Proc. Natl. Acad. Sci. U.S.A. **53**, 46 (1965).
[45] A. Girlando, A. Painelli, C. Pecile, G. Calestani, C. Rizzoli, and R. M. Metzger, J. Chem. Phys. **98**, 7692 (1993).
[46] M. Masino, A. Girlando, A. Brillante, R. G. D. Valle, E. Venuti, N. Drichko, and M. Dressel, Chem. Phys. **325**, 71 (2006).
[47] K. Takaoka, Y. Kaneko, H. Okamoto, Y. Tokura, T. Koda, T. Mitani, and G. Saito, Phys. Rev. B **36**, 3884 (1987).
[48] M. H. Lemee-Cailleau, M. LeCointe, H. Cailleau, T. Luty, F. Moussa, J. Roos, D. Brinkmann, B. Toudic, C. Ayache, and N. Karl, Phys. Rev. Lett. **79**, 1690 (1997).
[49] S. A. Bewick and Z. G. Soos, Chem. Phys. **325**, 60 (2006).
[50] W. H. Press, B. P. Flannery, S. A. Teukolsky, and W. T. Vetterling, *Numerical Recipes in Fortran 77* (Cambridge University Press, Cambridge, England, 1986).
[51] M. J. Rice and E. J. Mele, Phys. Rev. Lett. **49**, 1455 (1982).
[52] S. Kivelson, Phys. Rev. B **28**, 2653 (1983).
[53] Z. G. Soos and D. J. Klein, in *Treatise on Solid-State Chemistry*, edited by N. B. Hannay (Plenum Press, New York, 1976), Vol. III, p. 689.
[54] M. Buron-LeCointe, M. H. Lemee-Cailleau, H. Cailleau, B. Toudic, A. Moreac, F. Moussa, C. Ayache, and N. Karl, Phys. Rev. B **68**, 064103 (2003).
[55] M. LeCointe, M. H. Lemee-Cailleau, H. Cailleau, B. Toudic, L. Toupet, G. Heger, F. Moussa, P. Schweiss, K. H. Kraft, and N. Karl, Phys. Rev. B **51**, 3374 (1995).
[56] M. Masino and A. Girlando (private communication).
[57] T. Mitani, G. Saito, Y. Tokura, and T. Koda, Phys. Rev. Lett. **53**, 842 (1984).
[58] Z. G. Soos, D. Mukhopadhyay, A. Painelli, and A. Girlando, in *Handbook of Conducting Polymers*, 2nd ed., edited by T. Skotheim, R. Elsenbaumer, and J. Reynolds (Marcel Dekker, New York, 1998), p. 165.
[59] A. Gill, Contemp. Phys. **39**, 13 (1998).
[60] T. Luty, H. Cailleau, S. Koshihara, E. Collet, M. Takesada, M. H. Lemee-Cailleau, M. B.-L. Cointe, N. Nagaosa, Y. Tokura, E. Zienkiewicz, and B. Ouladdiaf, Europhys. Lett. **59**, 619 (2002).
[61] E. Collet, M. H. Lemee-Cailleau, M. B.-L. Cointe, H. Cailleau, S. Ravy, T. Luty, J. F. Berar, P. Czarnecki, and N. Karl, Europhys. Lett. **57**, 67 (2002).
[62] M. Buron-LeCointe, M. H. Lemee-Cailleau, H. Cailleau, S. Ravy, J. F. Berar, S. Rouziere, E. Elkaim, and E. Collet, Phys. Rev. Lett. **96**, 205503 (2006).
[63] T. Luty, in *Relaxations of Excited States and Photo-Induced Structural Phase Transitions*, Vol. 124 of Springer Series in Solid-State Sciences, edited by K. Nasu (Springer-Verlag, Berlin, 1996), p. 142.
[64] J. I. Kishine, T. Luty, and K. Yonemitsu, Phys. Rev. B **69**, 075115 (2004).
[65] K. Yonemitsu, Phys. Rev. B **73**, 155120 (2006).